CTSB mediates oxidative stress and intestinal epithelial barrier disruption in intestinal ischemia-reperfusion injury

SHUANG HE[1*], LEI WANG[2*], ZHE WANG[1*], SHIYONG YU[1], QI ZHU[1], YIJUN XU[1], YUHANG JIANG[1], YINGXIA WU[1] and HONGGANG XIANG[1]

[1]Department of General Surgery, Shanghai Pudong New Area People's Hospital, Shanghai 201299, P.R. China; [2]Department of General Surgery, Jinshazhou Hospital of Guangzhou University of Chinese Medicine, Guangzhou, Guangdong 510168, P.R. China

Received February 7, 2025; Accepted September 23, 2025

DOI: 10.3892/mmr.2025.13749

Abstract. Intestinal ischemia-reperfusion (I/R) injury is a clinical condition that leads to severe intestinal damage, inflammation and oxidative stress. While cathepsin B (*CTSB*) has been implicated in these pathophysiological processes, its precise role in mediating I/R-induced injury remains poorly understood. The present study aimed to elucidate how *CTSB* knockdown influences oxidative stress, inflammatory responses and the integrity of the intestinal epithelial barrier in intestinal epithelial Caco-2 cells subjected to I/R injury. To identify key genes implicated in I/R injury, a comprehensive analysis was conducted using differential expression profiling and protein-protein interaction network analysis of the GSE37013 dataset. To simulate I/R damage *in vitro*, an oxygen-glucose deprivation/reoxygenation (OGD/R) model was employed in Caco-2 cells. Subsequently, inflammation was induced by stimulating the cells with lipopolysaccharide (LPS) and adenosine triphosphate (ATP). To investigate the role of *CTSB* in this context, small interfering RNA was utilized to knock down *CTSB* expression. *In vitro* assays were then performed to evaluate NLR family pyrin domain-containing 3 (NLRP3) inflammasome activation, oxidative stress levels, inflammatory cytokine production and cell survival. The results revealed that intestinal tissues from the I/R group in the GSE37013 dataset showed markedly higher *CTSB* expression, and the Caco-2 cells subjected to OGD/R model resulted in a considerable increase in *CTSB* expression. However, the expression levels of tight junction proteins were enhanced, cell survival was improved and lactate dehydrogenase release was reduced by *CTSB* knockdown. This reduction in *CTSB* levels also reduced malondialdehyde levels, and alleviated oxidative stress by increasing the activities of glutathione peroxidase and superoxide dismutase. Furthermore, pro-inflammatory cytokine production was reduced, and NLRP3 inflammasome activation was inhibited by *CTSB* knockdown, although a modest increase was still observed after LPS + ATP stimulation. Notably, although *CTSB* knockdown significantly reduced the inflammatory response, LPS + ATP stimulation still elicited a modest reversal in cytokine levels, suggesting that a *CTSB*-independent pathway of inflammatory activation may exist. In conclusion, *CTSB* knockdown effectively mitigates I/R injury by reducing inflammation, preserving barrier integrity and alleviating oxidative stress, positioning *CTSB* as a promising therapeutic target. Future work should validate these findings in *in vivo* models and explore *CTSB*-targeted therapies to improve clinical outcomes in I/R-related diseases.

Introduction

Intestinal ischemia-reperfusion (I/R) injury represents a life-threatening condition precipitated by a transient interruption of blood flow to the intestines, followed by the abrupt restoration of circulation (1). This sequence of events triggers a cascade of detrimental effects, including oxidative stress, inflammation and apoptosis, all of which culminate in substantial tissue damage due to the sudden influx of oxygenated blood (2). I/R injury is frequently encountered in clinical scenarios such as organ transplantation or intestinal obstruction, where the restoration of blood supply, while intended to rescue tissue viability, often exacerbates cellular injury (3). Extensive investigations into the molecular mechanisms underlying I/R injury have revealed the involvement of multiple genes and signaling pathways in these pathological processes. Specifically, ferroptosis-induced intestinal tissue damage during I/R can be mitigated by inhibiting acyl-CoA synthetase long-chain family member 4 before reperfusion, highlighting the therapeutic potential of targeting ferroptosis-related genes (4). Additionally, it has been demonstrated that the activation of *JUN* and *FOS* transcription factors during I/R injury orchestrates a dual role, promoting both

Correspondence to: Dr Honggang Xiang or Dr Yingxia Wu, Department of General Surgery, Shanghai Pudong New Area People's Hospital, 490 Chuanhuan South Road, Pudong New Area, Shanghai 201299, P.R. China
E-mail: xianghonggang@shpdph.com
E-mail: wuyingxia@shpdph.com

*Contributed equally

Key words: intestinal ischemia-reperfusion, cathepsin B, oxidative stress, NLR family pyrin domain-containing 3 inflammasome, intestinal epithelial barrier disruption

apoptosis and compensatory cell proliferation, thereby underscoring the complexity of cellular responses to I/R stress (5). Furthermore, heme oxygenase-1 has emerged as a critical regulator of the oxidative stress response during I/R injury, with its induction serving as a protective mechanism against oxidative damage (6). Despite these advances, the complex interplay between signaling pathways implicated in I/R injury remains incompletely understood. Oxidative stress, a cornerstone of I/R-induced tissue damage, is orchestrated by a multitude of molecular factors, the interactions and cross-talk of which dictate the extent of cellular injury and recovery (7). Thus, further research is required to determine the complex regulatory networks governing I/R injury, with the aim of identifying novel therapeutic targets to mitigate tissue damage and improve clinical outcomes.

The lysosomal cysteine protease cathepsin B (*CTSB*) serves a role in various digestive system disorders. Studies have demonstrated that *CTSB* deficiency effectively mitigates symptoms linked to hypoxia-ischemia, inflammation and pain (8,9). For example, Xihuang pills have been shown to alleviate colitis by modulating *CTSB* levels, which in turn improve mucosal barrier integrity and suppress inflammation (10). Furthermore, Dong *et al* (11) revealed that administering mannose to treat inflammatory bowel disease (IBD) supports lysosomal stability and curtails *CTSB* release, thereby safeguarding against mitochondrial dysfunction during intestinal epithelial injury. Notably, *CTSB* serves as a mediator in the activation of NLR family pyrin domain-containing 3 (NLRP3) inflammasomes; it binds to NLRP3, thereby amplifying the activity of the NLRP3/caspase-1 inflammasome pathway (12). Research has indicated that colon inflammation induced by deoxycholic acid can be substantially diminished by inhibiting the NLRP3 inflammasome through the use of S1PR2 inhibitors and *CTSB* antagonists (13). Despite the progress made in understanding the involvement of *CTSB* in intestinal diseases, research regarding its function and underlying mechanisms in I/R-induced intestinal damage remains relatively limited. Th present study aimed to address this knowledge gap by exploring the role of *CTSB* in oxidative stress and disruption of the intestinal barrier during I/R injury.

In the setting of I/R injury, an overabundance of oxidative stress and inflammation represents a driving force behind epithelial barrier dysfunction, thereby intensifying cellular damage (14). Prior research has identified the pivotal role of *CTSB* in fostering inflammation and cell death in pathological states (15). Nevertheless, its precise contribution to I/R-triggered intestinal injury has been relatively under-investigated. The present study aimed to assess the effects of *CTSB* knockdown on alleviating oxidative stress, mitigating intestinal barrier impairment and curbing NLRP3 inflammasome activation in Caco-2 cells subjected to oxygen-glucose deprivation/reoxygenation (OGD/R). The results of this investigation may provide novel insights into the therapeutic promise of targeting *CTSB* for the management of I/R injury.

Materials and methods

Screening of datasets and identification of differentially expressed genes (DEGs). For in-depth analysis, the GSE37013 dataset was accessed from the Gene Expression Omnibus (https://www.ncbi.nlm.nih.gov/geo/) repository, originally reported by Kip *et al* (16). This dataset comprises 28 samples, including seven non-ischemic surgical control jejunal samples collected intraoperatively and 21 I/R case samples. Differential expression analysis on the GSE37013 dataset was conducted using the limma package (version 3.48.3; https://bioconductor.org/packages/limma) implemented in R (version 4.1.2; R Foundation for Statistical Computing; https://www.r-project.org/). Genes exhibiting a fold change (FC) of >1.3 were categorized as upregulated, whereas those with an FC of <0.77 were deemed downregulated; $P<0.05$ was employed to denote a statistically significant difference. To visualize the DEGs, the ggplot2 package (https://cran.r-project.org/package=ggplot2) was utilized in R.

Expression validation of overlapping genes in protein-protein interaction (PPI) networks. To elucidate the interactions among DEGs, a PPI network analysis was conducted using the Search Tool for the Retrieval of Interacting Genes (https://string-db.org/). The top 15 genes were identified using the Cytohubba plugin within Cytoscape (version 3.9.1; https://cytoscape.org), employing algorithms such as the maximum neighborhood component (MNC), maximal clique centrality (MCC) and degree. Subsequently, an intersection analysis was performed on the top 15 genes derived from these three network modules using the Bioinformatics and Evolutionary Genomics online tool (http://bioinformatics.psb.ugent.be/webtools/Venn/). The gene expression levels of the intersection genes in both the control and case groups of the GSE37013 dataset were then analyzed using the SangerBox platform (http://sangerbox.com/). $P<0.05$ was deemed statistically significant for the scores obtained in this analysis.

Cell culture. Caco-2 cells, from a human colorectal adenocarcinoma, were sourced from National Collection of Authenticated Cell Cultures. These cells were cultured in DMEM (Procell Life Science & Technology Co., Ltd.), supplemented with 10% fetal bovine serum (Procell Life Science & Technology Co., Ltd.) and 1% penicillin-streptomycin solution (Procell Life Science & Technology Co., Ltd.). Cell culture was performed at 37˚C within a humidified incubator maintained at 5% CO_2.

I/R and inflammation models. An OGD/R model was established to simulate I/R injury. The cells were subjected to OGD/R by being incubated in glucose-free DMEM at 37˚C within a microaerobic environment (comprising 1% O_2, 94% N_2, 5% CO_2) for varying durations of 0, 2, 4 and 6 h. Subsequently, the cells underwent reoxygenation in complete DMEM under normoxia at 37˚C (21% O_2, 5% CO_2, 74% N_2) for 24 h. Control cells were maintained in complete DMEM (with glucose and 10% FBS) at 37˚C under normoxia (21% O_2, 5% CO_2, balance N_2) and underwent the same medium-change schedule as the OGD/R groups. Additionally, to induce inflammation, Caco-2 cells (which had been treated with OGD for 4 h followed by reoxygenation for 24 h) were exposed to 1 μg/ml lipopolysaccharide (LPS; Beijing Solarbio Science & Technology Co., Ltd.) for 6 h at 37˚C. Finally, adenosine triphosphate (ATP; Beyotime Institute of Biotechnology) was introduced at a concentration of 5 mM and the cells were incubated for 30 min at 37˚C.

Cell transfection. Transfection was performed after OGD/R. After seeding at a density of $2x10^5$ cells/well in 6-well plates, Caco-2 cells were cultured until they reached 60-70% confluence. To achieve knockdown of *CTSB*, the cells were transfected with specific small interfering RNA (siRNA; final concentration, 50 nM) designed to target *CTSB*, adhering strictly to the manufacturer's protocol. The transfection was carried out using 10 μl Lipofectamine™ 2000 reagent (Invitrogen; Thermo Fisher Scientific, Inc.) at 37˚C for 6 h. As a negative control (NC), a non-targeting siRNA was employed. Following transfection, the cells were incubated for an additional 48 h before being harvested for use in further experiments. The siRNA sequences utilized for transfection were as follows: si-*CTSB*, sense 5'-CCUGUCGGAUGAGCU GGUCAACU-3', antisense 5'-AUAGUUGACCAGCUCAUC GACAG-3'; si-NC, sense 5'-CCUAGCGAGUGGUCAACU GUAU-3', antisense 5'-AUACAGAGUUGACCACUCGCC UAG-3'.

Assessment of Caco-2 cell viability. The Cell Counting Kit-8 (CCK-8) assay (Beyotime Institute of Biotechnology) was utilized to evaluate cell viability, according to the manufacturer's instructions. Initially, 96-well plates were seeded with $5x10^3$ Caco-2 cells/well in 100 μl complete growth medium. The plates were then incubated overnight at 37˚C in a humidified incubator maintained at 5% CO_2, allowing the cells to adhere and achieve a stable growth state. Following this incubation period, each well was supplemented with 10 μl CCK-8 solution, and the plates were further incubated for 2 h at 37˚C. Subsequently, cell viability was assessed by measuring the absorbance at 450 nm using a microplate reader (Bio-Rad Laboratories, Inc.). To ensure the robustness and reliability of the findings, data from a minimum of three independent experiments were subjected to statistical analysis.

Detection of lactate dehydrogenase (LDH) levels. Caco-2 cells were exposed to OGD for 2, 4 and 6 h, followed by 24 h of reoxygenation to evaluate the resultant impact on LDH levels. According to the manufacturer's guidelines, culture supernatants were carefully collected, and LDH levels were measured using an LDH cytotoxicity assay kit (Beyotime Institute of Biotechnology). To ensure the reliability of the data, the assay was conducted in triplicate for each time point. LDH activity was quantified by recording the absorbance at 490 nm using a microplate reader. Data obtained from a minimum of three independent experiments were subjected to rigorous statistical analysis to discern the significance of the differences in LDH levels across the various OGD/R treatment durations.

Reverse transcription-quantitative PCR (RT-qPCR). Total RNA was extracted from Caco-2 cells using TRIzol® reagent (Invitrogen; Thermo Fisher Scientific, Inc.) according to the manufacturer's detailed instructions, after the aforementioned OGD/R and/or LPS/ATP treatments. Subsequently, 1 μg isolated total RNA was reverse-transcribed into cDNA utilizing the PrimeScript RT reagent kit (Takara Biotechnology, Ltd.) according to the manufacturer's protocol. qPCR was performed on a Bio-Rad CFX96 Real-Time PCR Detection System (Bio-Rad Laboratories, Inc.), employing the SYBR Green kit (Takara Biotechnology, Ltd.). The expression levels of the target genes, as well as the internal control GAPDH, were quantified using gene-specific primers (Table I). The thermocycling conditions were as follows: 95˚C for 30 sec, followed by 40 cycles at 95˚C for 5 sec and 60˚C for 30 sec; a melt-curve analysis was then performed from 65-95˚C with 0.5˚C increments. The relative expression of each candidate gene was determined using the $2^{-\Delta\Delta Cq}$ method (17). To ensure the robustness of the findings, data from a minimum of three independent experiments were subjected to statistical analysis.

Western blot (WB) analysis. To lyse Caco-2 cells, RIPA lysis buffer (Beyotime Institute of Biotechnology) was prepared with the addition of protease and phosphatase inhibitors. The total protein content in the lysates was then quantified using a BCA protein assay kit (Beyotime Institute of Biotechnology). Equal amounts of protein (20 μg) were separated by SDS-PAGE on 10% polyacrylamide gels and were subsequently transferred onto PVDF membranes (Beyotime Institute of Biotechnology). To prevent non-specific binding, the membranes were blocked for 1 h at room temperature with 5% skim milk dissolved in Tris-buffered saline containing 0.1% Tween-20 (TBST). To detect the target proteins, the antibodies for each target protein and the internal control GAPDH antibody were mixed separately, and the PVDF membranes were incubated with the primary antibody solutions at 4˚C overnight. The following primary antibodies were used: CTSB (cat. no. 12216-1-AP; 1:1,000; Wuhan Sanying Biotechnology), active CTSB (cat. no. 12216-1-AP; 1:1,000; Wuhan Sanying Biotechnology), ZO-1 (cat. no. ab276131; 1:1,000; Abcam), claudin-1 (cat. no. ab211737; 1:2,000; Abcam), NLRP3 (cat. no. 30109-1-AP; 1:2,000; Wuhan Sanying Biotechnology), gasdermin D (GSDMD; cat. no. ab210070; 1:1,000; Abcam), cleaved N-terminal GSDMD (GSDMD-N; cat. no. ab215203; 1:2,000; Abcam), ASC (cat. no. 10500-1-AP; 1:5,000; Wuhan Sanying Biotechnology), cleaved caspase-1 (p20; cat no. AF4005; 1:2,000; Affinity Biosciences), caspase-1 (cat. no. ab207802; 1:1,000; Abcam), IL-1β (cat. no. ab283818; 1:1,000; Abcam), IL-18 (cat. no. 82696-15-RR; 1:2,000; Wuhan Sanying Biotechnology) and GAPDH (cat. no. 80570-1-RR; 1:2,500; Wuhan Sanying Biotechnology). After washing the membranes three times with TBST, they were incubated for 1 h at room temperature with HRP-conjugated goat anti-rabbit IgG (cat. no. A0208; 1:1,000; Beyotime Institute of Biotechnology). Protein bands were detected using an enhanced chemiluminescence detection system (Bio-Rad Laboratories, Inc.). Band intensities were semi-quantified using ImageJ software (version 2.0.0; National Institutes of Health). To ensure accurate normalization, the bands of both the proteins of interest and GAPDH were developed from the same membrane, subjected to the same blocking, incubation and washing steps, and visualized under identical conditions.

Co-immunoprecipitation (Co-IP). To investigate the interaction between CTSB and NLRP3, co-IP was employed. Cells were harvested and lysed in RIPA buffer (Beyotime Institute of Biotechnology) supplemented with a protease-inhibitor cocktail. Lysates were clarified at 12,000 x g for 10 min at 4˚C, and protein concentrations were determined by BCA assay. The resulting cell lysates were then mixed with 30 μl protein A/G agarose bead slurry (Santa Cruz Biotechnology,

Table I. Primer sequences for reverse transcription-quantitative PCR.

Target	Sequence, 5'-3'
CTSB	F: GTACACCTGCGAGTGTTCCA
	R: CAAGTGCACGCTCTGGTAGA
ZO-1	F: CTCAAGAGGAAGCTGTGGGT
	R: CCATTGCTGTGCTAGTGAGC
CLDN1	F: ATGACCCCAGTCAATGCCAG
	R: GCTGGAAGGTGCAGGTTTTG
TNF-α	F: CACAGTGAAGTGCTGGCAAC
	R: AGGAAGGCCTAAGGTCCACT
IL-6	F: TTCGGTCCAGTTGCCTTCTC
	R: CTGAGATGCCGTCGAGGATG
IL-1β	F: AGCCATGGCAGAAGTACCTG
	R: GAAGCCCTTGCTGTAGTGGT
GAPDH	F: CATGTTGCAACCGGGAAGGA
	R: ATCACCCGGAGGAGAAATCG

CTSB, cathepsin B; *CLDN1*, claudin-1; F, forward; R, reverse.

Inc.) per 1 mg total protein for 1 h at 4˚C on a rotator to remove non-specific binding. Following centrifugation (2,500 x g, 3 min, 4˚C), the agarose beads were discarded, and the supernatant, containing the pre-cleared lysates, was collected. Primary antibodies specific for either CTSB (cat. no. ab30443; Abcam) or NLRP3 (cat. no. 30109-1-AP; Wuhan Sanying Biotechnology), or an equal amount of species-matched normal IgG (negative control), were added at 2 μg per IP and mixtures were incubated for 6 h at 4˚C on a rotator to allow antigen-antibody binding. Subsequently, an additional 30 μl protein A/G agarose beads was added, and the suspensions were rotated overnight at 4˚C to capture the antigen-antibody complexes. Beads were collected by centrifugation (2,500 x g, 3 min, 4˚C) and washed four times with ice-cold RIPA lysis buffer (1 ml/wash) to remove any unbound proteins. The antigen-antibody complexes were eluted from the beads using 2X Laemmli SDS sample buffer at 95˚C for 5 min. The eluate was boiled and denatured to prepare it for subsequent WB analysis.

Enzyme-linked immunosorbent assay (ELISA). ELISA was carried out to quantify CTSB, TNF-α, IL-6 and IL-1β using the following commercially available kits: Human CTSB ELISA Kit (cat. no. ab119584; Abcam), Human TNF-αELISA Kit (cat. no. BMS2034; Invitrogen; Thermo Fisher Scientific, Inc.), Human IL-6 ELISA Kit (cat. no. EH2IL6; Invitrogen; Thermo Fisher Scientific, Inc.), and Human IL-1β Instant ELISA Kit (cat. no. BMS224INST; Invitrogen; Thermo Fisher Scientific, Inc.) according to the manufacturer's instructions. For each assay, 100 μl Caco-2 cell culture supernatant/well was carefully transferred to pre-coated 96-well plates, and the plates were incubated according to the manufacturer's guidelines. The enzymatic reaction was developed using the tetramethylbenzidine substrate, and the absorbance at 450 nm was measured using a microplate reader. Protein concentrations were calculated based on standard curves generated with kit-supplied standards. To ensure the robustness and reliability of the results, each experiment was replicated at least three times. Data from these independent experiments were subjected to statistical analysis to evaluate the significance of differences in protein levels between experimental groups.

Immunofluorescence analysis. After OGD for 4 h followed by 24 h reoxygenation, cells were fixed for 15 min at room temperature in 4% paraformaldehyde solution. Subsequently, the cells were permeabilized for 10 min with 0.1% Triton X-100 to facilitate antibody penetration and then blocked for 1 h with 5% bovine serum albumin (BSA; Beyotime Institute of Biotechnology) dissolved in phosphate-buffered saline (PBS) to mitigate non-specific binding. Primary antibodies targeting ZO-1 (cat. no. ab276131; 1:500) and claudin-1 (cat. no. ab211737; 1:1,000) (both from Abcam) were diluted in 1% BSA and incubated with the cells overnight at 4˚C to allow for specific antigen-antibody interactions. The following day, the cells were incubated with Alexa Fluor® 488-labeled goat anti-rabbit IgG secondary antibodies (cat. no. A-11008; 1:1,000; Invitrogen; Thermo Fisher Scientific, Inc.) for 1 h at room temperature in the dark to preserve the fluorescence signal. The nuclei were counterstained DAPI (Beyotime Institute of Biotechnology) for 5 min at room temperature after washing with PBS. Fluorescence microscopy images were captured using a fluorescence microscope (Nikon Eclipse Ti-U; Nikon Corporation). To ensure the reproducibility and reliability of our findings, the entire immunofluorescence staining protocol was replicated at least three times, with three technical replicates per condition in each experiment.

Oxidative stress markers assay. After 4 h of OGD followed by 24 h of reoxygenation, cells were lysed on ice using the kit-supplied sample lysis buffer (Beyotime Institute of Biotechnology). The lysates were subsequently analyzed using commercially available detection kits for reactive oxygen species (ROS; cat. no. S0033S), malondialdehyde (MDA; cat. no. S0131S), superoxide dismutase (SOD; cat. no. S101S) and glutathione peroxidase (GSH-Px; cat. no. S0059S) (all from Beyotime Institute of Biotechnology). These assays were conducted according to the manufacturer's instructions. Absorbance values were recorded using a microplate reader at the following specific wavelengths: 488 nm (excitation) and 525 nm (emission) for ROS, 412 nm for GSH-Px, 450 nm for SOD and 532 nm for MDA. To ensure the reliability and reproducibility of the data, each test was performed in triplicate.

Statistical analysis. All results are presented as the mean ± standard deviation. To determine statistical significance, one-way analysis of variance was utilized, followed by Tukey's post hoc test for multiple comparisons between groups. For pairwise comparisons between two specific groups, a two-tailed unpaired Student's t-test was employed. $P<0.05$ was considered to indicate a statistically significant difference. All statistical analyses were conducted using the R programming language. Additionally, graphs were generated exclusively for visualization purposes using GraphPad Prism software (version 8.0; Dotmatics) to facilitate interpretation of the results.

Results

Differential expression and PPI network analysis to obtain key intersection genes. First, a differential expression analysis was conducted using the GSE37013 dataset, comparing I/R jejunal samples (n=21) with non-ischemic surgical controls (n=7), which yielded 181 downregulated and 224 upregulated DEGs (Fig. 1A). Subsequently, a PPI network analysis was performed on the DEGs. This analysis revealed the top 15 genes as identified by three different algorithms: Degree (15 nodes and 44 edges; Fig. 1B), MCC (15 nodes and 50 edges; Fig. 1C) and MNC (15 nodes and 52 edges; Fig. 1D). Following this, a cross-analysis of the top 15 genes from each of the three algorithms was conducted, resulting in the identification of 13 key intersection genes (Fig. 1E). Expression analysis was then performed to examine the expression levels of these genes in both the control and case samples from the GSE37013 dataset (Fig. 1F). The results demonstrated that in the case samples, *BIRC3*, *CTSB*, *EZH2*, *GSK3B*, *LAMP1*, *PTPRC* and *TLR3* were significantly upregulated, whereas *EGFR*, *NCAM1*, *PLCG1*, *SQSTM1*, *STAT5B* and *ZAP70* were significantly downregulated.

OGD/R decreases cell viability, disrupts tight junction protein expression and increases CTSB activity. The current study assessed the effects of OGD/R on the expression of tight junction proteins and CTSB, LDH release and cell survival in Caco-2 cells. Compared with in the control group, as the duration of OGD/R treatment was extended, the results from the CCK-8 assay revealed a progressive decline in cell viability (Fig. 2A). Concurrently, a significant increase in LDH levels was observed with prolonged OGD/R exposure (Fig. 2B). Furthermore, following OGD/R treatment, there was a gradual decrease in the mRNA expression levels of *ZO-1* and *CLDN1*, with their levels declining progressively as the duration of OGD/R exposure increased (Fig. 2C and D). Based on preliminary experiments (Fig. 2A and B), which demonstrated significant but sub-lethal injury at the 4-h OGD mark, consistent with established *in vitro* I/R models (18), subsequent experiments used the same 4-h OGD treatment to further examine its effect on CTSB activity. Subsequently, an ELISA was employed to examine CTSB activity in Caco-2 cells. In the OGD/R model, CTSB activity was markedly elevated compared with that in the control group (Fig. 2E). WB analysis further confirmed that both total CTSB protein and active CTSB protein levels were increased following OGD/R treatment (Fig. 2F and G).

CTSB knockdown alleviates OGD/R-induced Caco-2 cell injury. RT-qPCR and WB analysis confirmed the efficient knockdown of *CTSB*, resulting in a significant reduction in CTSB expression following transfection (Figs. S1 and 3A-C). To evaluate the impact of *CTSB* knockdown on the viability of Caco-2 cells exposed to OGD/R, the CCK-8 assay was employed. OGD/R resulted in a marked reduction in cell viability compared with that in the control group, whereas *CTSB* knockdown effectively reversed this reduction, thereby preserving cell viability (Fig. 3D). Furthermore, LDH levels, which serve as an indicator of cell damage, were markedly elevated in the OGD/R-treated cells; however, *CTSB* knockdown notably reduced LDH release, suggesting a decrease in cellular injury (Fig. 3E). WB analysis results further revealed that the protein levels of ZO-1 and claudin-1, both of which were reduced in the OGD/R model, were restored following *CTSB* knockdown (Fig. 3F and G). Immunofluorescence staining provided additional confirmation, demonstrating the recovery of ZO-1 and claudin-1 expression after *CTSB* knockdown (Fig. 3H and I). Collectively, these findings suggested that *CTSB* knockdown may mitigate I/R-induced cellular injury and preserve epithelial barrier integrity in Caco-2 cells.

CTSB knockdown alleviates OGD/R-induced oxidative stress and inflammatory response. To elucidate the role of *CTSB* in oxidative stress and inflammatory responses within I/R-injured Caco-2 cells, a series of experiments were conducted. The levels of ROS in the OGD/R model, as assessed using an assay kit, were significantly higher than those in the control group, indicating an increase in oxidative stress (Fig. 4A). Notably, *CTSB* knockdown attenuated this elevation in ROS levels, suggesting that *CTSB* serves an important role in regulating oxidative stress. Furthermore, MDA levels, evaluated using an MDA detection kit, were markedly elevated in the OGD/R model group compared with those in the control group, whereas *CTSB* knockdown mitigated this increase (Fig. 4B), indicating a reduction in lipid peroxidation. SOD activity, which was markedly decreased in the OGD/R model group, was partially restored following *CTSB* knockdown (Fig. 4C), suggesting an enhancement in antioxidative capacity. Similarly, GSH-Px activity, which was significantly decreased in the OGD/R model group, was reversed by *CTSB* knockdown (Fig. 4D), further supporting its role in oxidative stress regulation. The results of ELISA revealed that the OGD/R model group exhibited higher levels of pro-inflammatory cytokines, including IL-6, IL-1β and TNF-α; by contrast, *CTSB* knockdown significantly reduced the levels of these inflammatory markers (Fig. 4E-G). Collectively, these findings suggested that *CTSB* knockdown may alleviate oxidative stress and inflammatory responses in Caco-2 cells following I/R injury, thereby highlighting the potential therapeutic benefits of targeting CTSB in this context.

CTSB knockdown attenuates OGD/R-induced NLRP3 inflammasome activation and proinflammatory cytokine expression. To investigate the role of *CTSB* in the inflammatory responses induced by OGD/R in Caco-2 cells, the expression of key inflammasome components and pro-inflammatory cytokines was examined. WB analysis revealed that OGD/R treatment significantly elevated the protein expression levels of GSDMD-N, NLRP3, ASC, cleaved caspase-1, IL-1β and IL-18 compared with those in the control group (Fig. 5A-D). However, *CTSB* knockdown effectively reduced the protein levels of these inflammatory mediators. Given the pivotal role of *CTSB* in the inflammatory process, the current study aimed to explore whether CTSB directly interacts with NLRP3, a key component of the inflammasome. Notably, a previous study has suggested an interaction exists between CTSB and NLRP3 (11). To further investigate this, co-IP experiments were conducted. The results confirmed that CTSB interacts with NLRP3 in the intestinal I/R model (Fig. 5E and F). When CTSB was immunoprecipitated (Fig. 5E), NLRP3 was

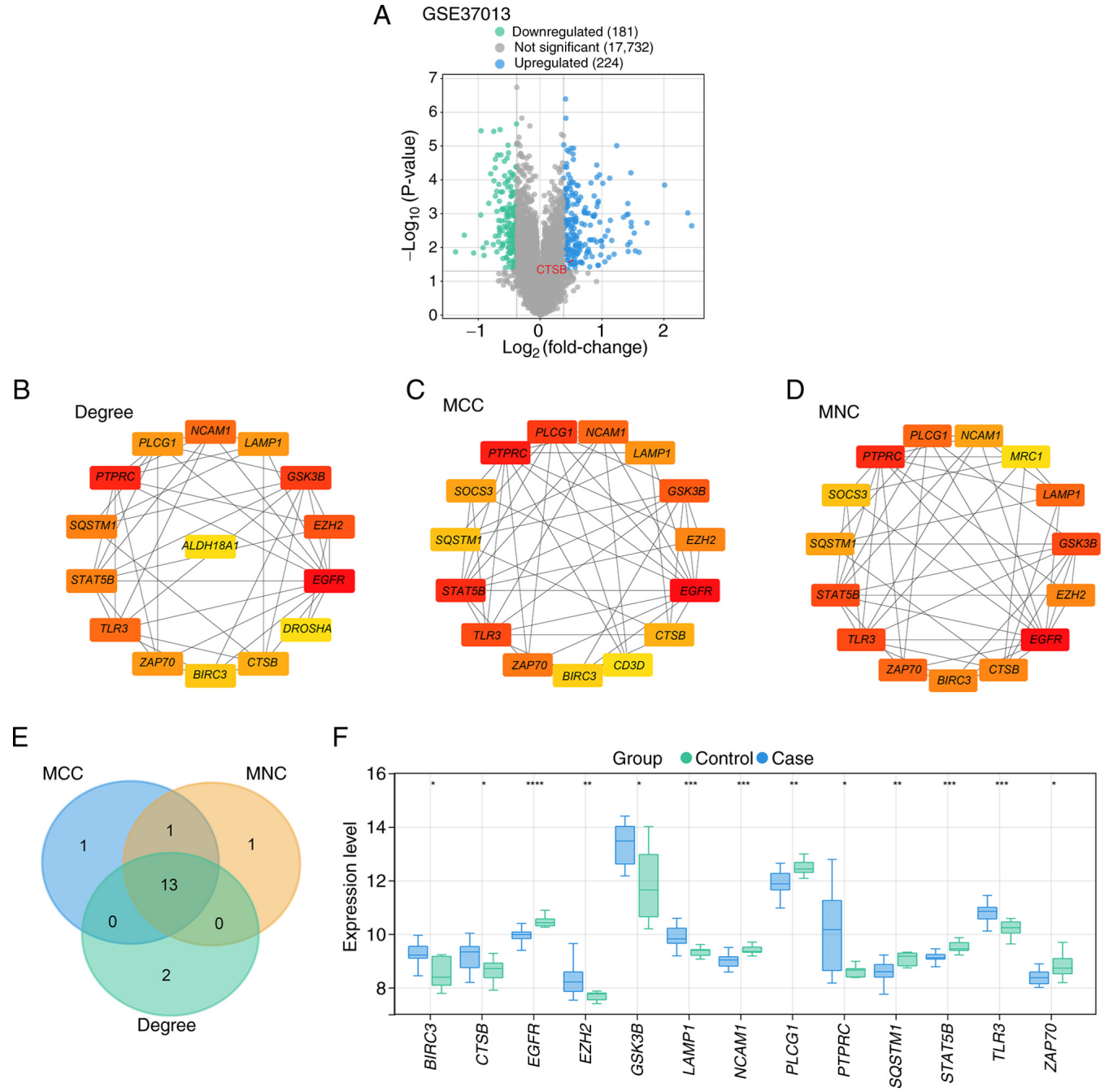

Figure 1. Screening of DEGs, PPI network construction and intersection analysis based on the GSE37013 dataset to identify hub genes. (A) Volcano plot of DEGs in the GSE37013 dataset. Green represents 181 downregulated DEGs and blue represents 224 upregulated DEGs. PPI network analysis of upregulated DEGs using (B) degree, (C) MCC and (D) MNC algorithms, and visualization of the top 15 genes in each network. (E) Venn diagram of the intersection analysis of the top 15 genes of the degree, MCC and MNC algorithms, where the overlapping genes represent the intersection genes. (F) Box plot of the expression levels of 13 intersection genes in control and case samples from the GSE37013 dataset. *P<0.05, **P<0.01, ***P<0.001, ****P<0.0001. *CTSB*, cathepsin B; DEG, differentially expressed gene; MCC, maximal clique centrality; MNC, maximum neighborhood component; PPI, protein-protein interaction.

detected only in the OGD/R + si-NC group. This is consistent with the strong induction of NLRP3 by OGD/R and its marked reduction after *CTSB* silencing, rendering the co-precipitated NLRP3 in the control and OGD/R + si-*CTSB* groups below the detection limit. Conversely, when NLRP3 was immunoprecipitated (Fig. 5F), CTSB was recovered in all groups because CTSB is constitutively expressed, with the signal highest in the OGD/R + si-NC groups and decreased after *CTSB* knockdown. These reciprocal co-IP findings support a specific CTSB-NLRP3 interaction in this model. Furthermore, OGD/R treatment significantly elevated the mRNA expression levels of pro-inflammatory cytokines (Fig. 5G-5I), whereas *CTSB* knockdown markedly decreased the expression levels of these cytokines. Notably, when cells were further treated with LPS and ATP following *CTSB* knockdown, cytokine expression was partially restored, suggesting a CTSB-independent pathway of inflammatory activation.

CTSB knockdown alleviates OGD/R-induced oxidative stress and impaired intestinal barrier function. Compared with

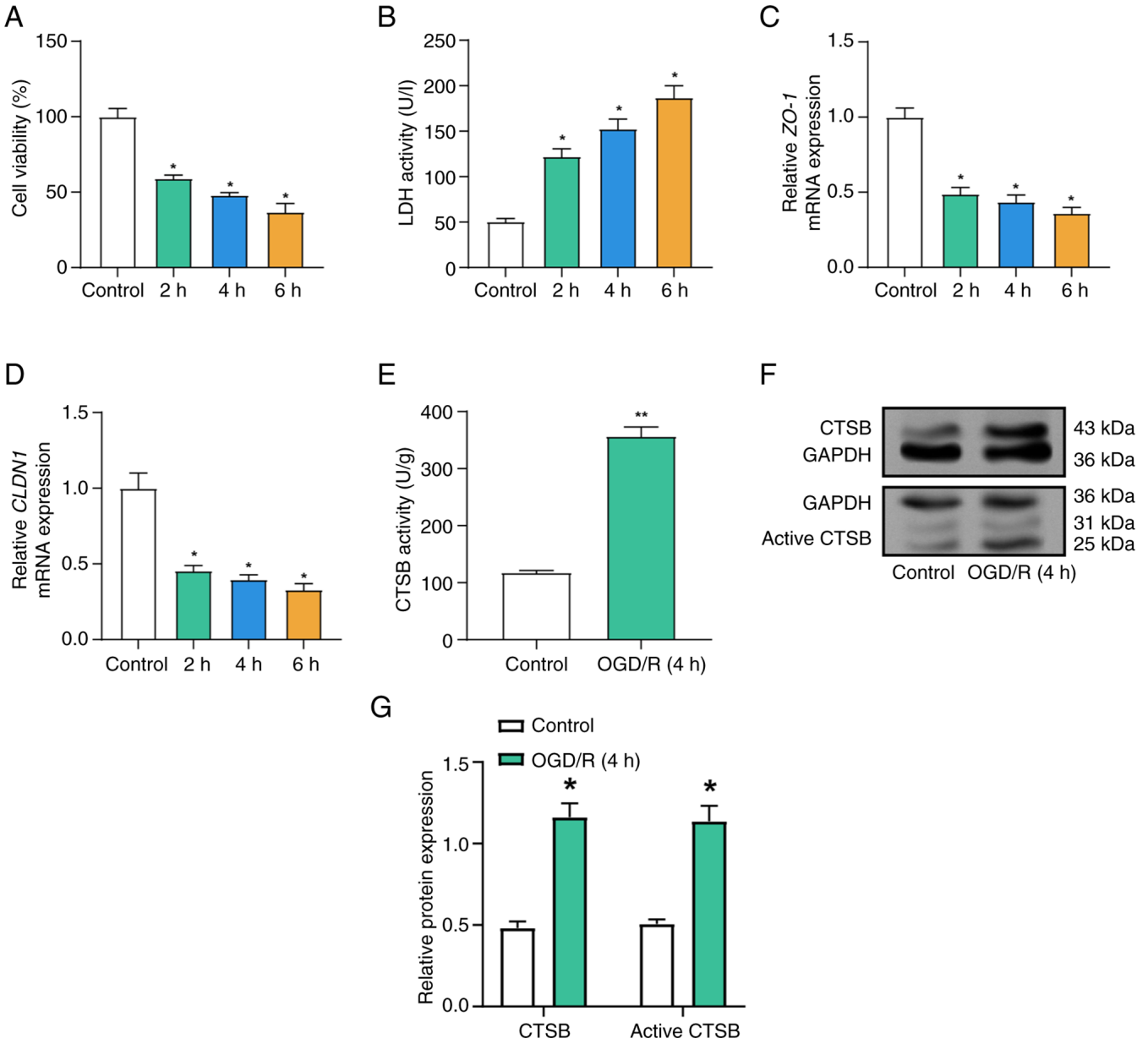

Figure 2. *CTSB* expression is elevated in intestinal barrier damage induced by ischemia-reperfusion. (A) Cell Counting Kit-8 detected the viability of Caco-2 cells in the control and OGD/R-treated (2, 4 and 6 h) groups. (B) LDH activity detection in Caco-2 cells from the control and OGD/R-treated (2, 4 and 6 h) groups. Reverse transcription-quantitative PCR was used to detect the relative mRNA expression levels of (C) *ZO-1* and (D) *CLDN1* in Caco-2 cells in the control and OGD/R-treated (2, 4 and 6 h) groups. (E) Enzyme-linked immunosorbent assay detected CTSB activity in Caco-2 cells in the control and OGD/R-treated (4 h) groups. (F) Western blot analysis was used to detect the protein expression levels of CTSB and active CTSB in Caco-2 cells in the control and OGD/R-treated (4 h) groups, and (G) semi-quantitative analysis was performed. All data were obtained from at least three independent biological experiments (n=3). *P<0.05, **P<0.01 vs. control. CLDN1, claudin-1; CTSB, cathepsin B; LDH, lactate dehydrogenase; OGD/R, oxygen-glucose deprivation/reoxygenation.

those in the control group, WB analysis demonstrated that OGD/R treatment significantly reduced the expression levels of tight junction proteins, specifically ZO-1 and claudin-1 (Fig. 6A and B). However, *CTSB* knockdown significantly restored these protein levels. Notably, further treatment with LPS and ATP following *CTSB* knockdown partially reversed this recovery, suggesting a regulatory role of CTSB in maintaining tight junction integrity under inflammatory conditions. This suggests that LPS and ATP may counteract the benefits of *CTSB* knockdown. The results of the cell viability experiment indicated a substantial decrease in cell viability following OGD/R treatment compared with that in the control group (Fig. 6C). By contrast, *CTSB* knockdown significantly enhanced cell viability under OGD/R conditions, indicating its protective effect; however, the subsequent addition of LPS and ATP attenuated this protective effect, suggesting that LPS and ATP may counteract the benefits of *CTSB* knockdown. Subsequently, it was revealed that MDA levels in OGD/R-treated cells were significantly elevated, indicating an increase in oxidative stress (Fig. 6D). By contrast, *CTSB* knockdown significantly reduced MDA levels, demonstrating its antioxidant potential; however, treatment with LPS and ATP partially reversed this decrease, suggesting that LPS and ATP may exacerbate oxidative stress despite *CTSB*

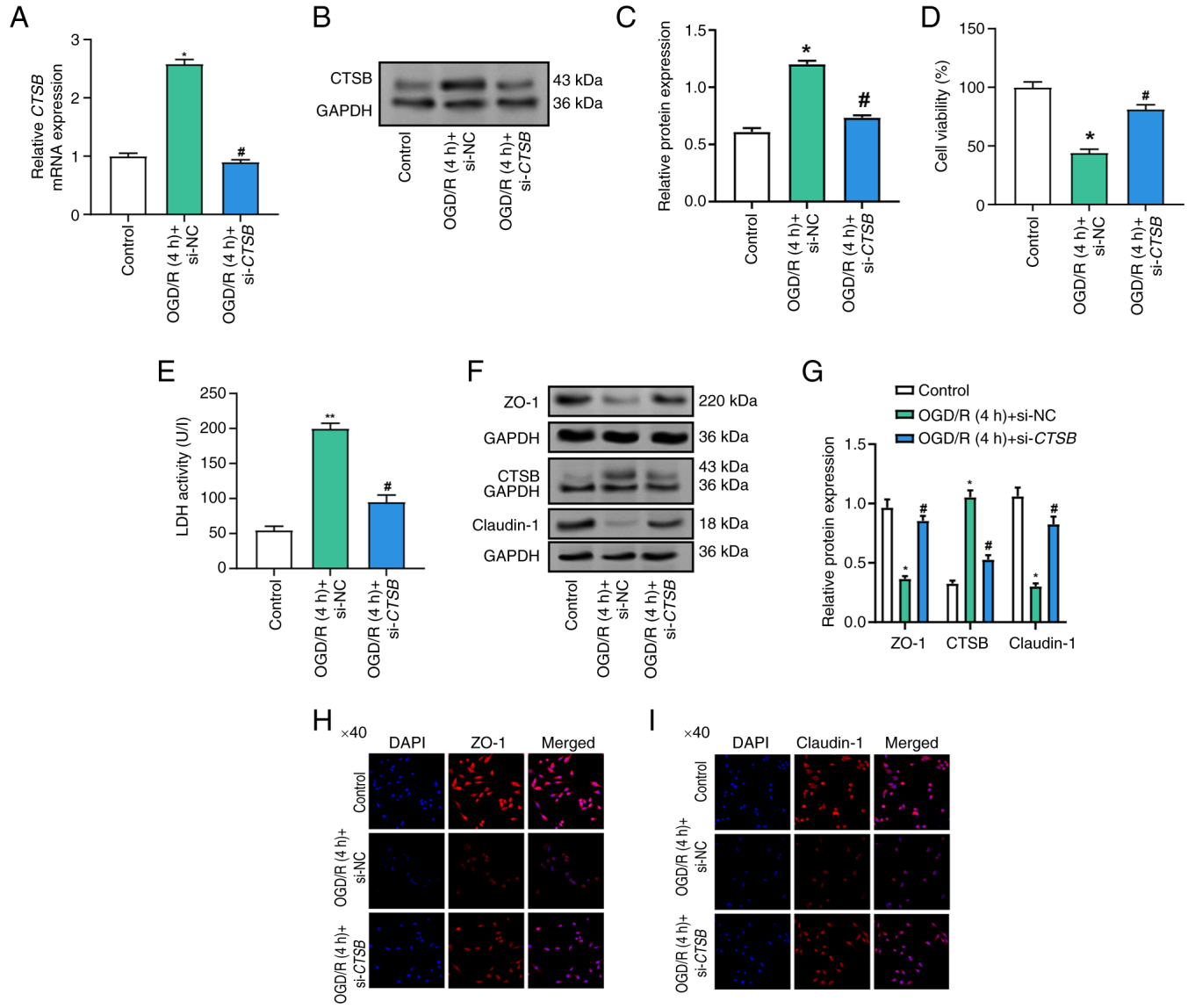

Figure 3. Effects of *CTSB* knockdown on cell viability, LDH activity and tight junction protein expression in OGD/R-treated Caco-2 cells. (A) Reverse transcription-quantitative PCR analysis of the relative expression levels of *CTSB* mRNA in the control group, the OGD/R + si-NC group and the OGD/R + si-*CTSB* group. (B) Representative western blot of CTSB protein in the Control, OGD/R + si-NC and OGD/R + si-*CTSB* groups. GAPDH was used as the loading control. (C) Densitometric semi-quantification of CTSB protein expression (normalized to GAPDH). (D) Cell Counting Kit-8 detected the viability of Caco-2 cells in the control, OGD/R (4 h) + si-NC and OGD/R (4 h) + si-*CTSB* groups. (E) LDH activity of Caco-2 cells was detected in the control, OGD/R (4 h) + si-NC and OGD/R (4 h) + si-*CTSB* groups. (F) WB analysis of the protein expression of CTSB, ZO-1 and claudin-1 in control, OGD/R (4 h) + si-NC and OGD/R (4 h) + si-*CTSB* Caco-2 cell groups, and (G) semi-quantitative analysis. Immunofluorescence analysis of (H) ZO-1 and (I) claudin-1 in Caco-2 cells in the control, OGD/R (4 h) + si-NC, and OGD/R (4 h) + si-*CTSB* groups. Magnification, x40. All data were obtained from at least three independent biological experiments (n=3). *P<0.05, **P<0.01 vs. control; $^{\#}$P<0.05 vs. OGD/R (4 h) + si-NC. CTSB, cathepsin B; LDH, lactate dehydrogenase; NC, negative control; OGD/R, oxygen-glucose deprivation/reoxygenation; si, small interfering; WB, western blot.

knockdown. Furthermore, OGD/R-treated cells exhibited a substantial reduction in SOD activity, which was restored by *CTSB* knockdown (Fig. 6E). Notably, the protective impact of *CTSB* knockdown on SOD activity was, however, diminished by subsequent LPS and ATP treatment, further emphasizing the complex interplay between *CTSB*, inflammation and oxidative stress.

Discussion

I/R injury represents a complex pathogenic process that arises from the transient interruption of blood flow, followed by the reintroduction of oxygen to tissues; this sequence of events precipitates cellular damage and inflammation (19). Previous studies have identified the critical molecular mediators in I/R injury, elucidating their roles in amplifying tissue destruction and inflammatory responses. For example, research has demonstrated the involvement of microRNAs (miRs) in I/R. Specifically, the overexpression of miR-146a-5p has been shown to target *TXNIP*, modulating the PRKAA/mTOR pathway, which in turn inhibits autophagy and mitigates intestinal barrier damage (20). Through rigorous bioinformatics analysis, the present study identified several genes that exhibit significant differential expression in the context of I/R injury. Some of these genes have already been validated in prior studies for their association with I/R. For example, *PTPRC*

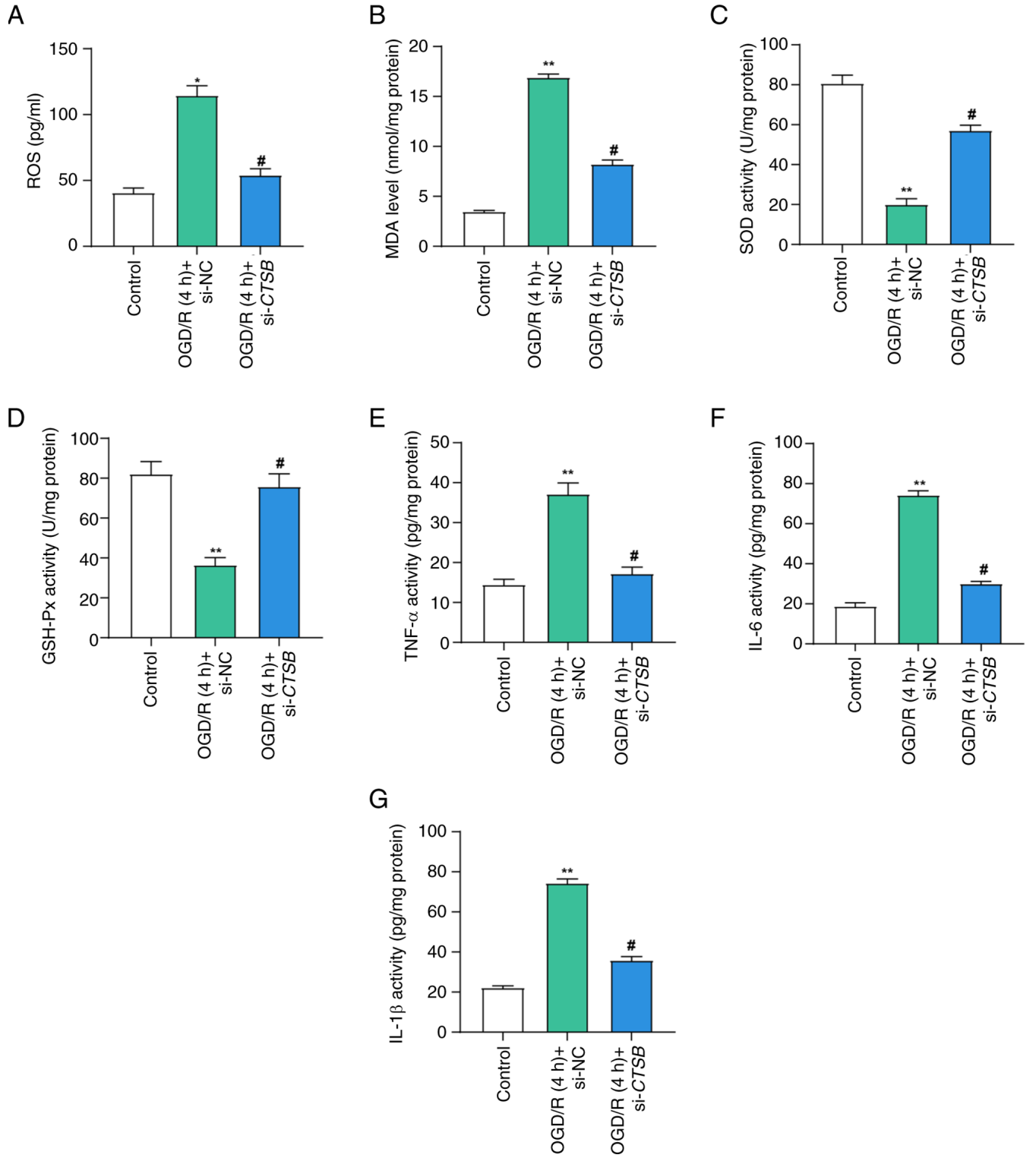

Figure 4. *CTSB* knockdown mitigates ischemia-reperfusion-induced oxidative stress and inflammation. Detection of (A) ROS levels, (B) MDA levels, (C) SOD activity and (D) GSH-Px activity in Caco-2 cells in the control, OGD/R (4 h) + si-NC and OGD/R (4 h) + si-*CTSB* groups. Enzyme-linked immunosorbent assay detected the activities of the cytokines (E) TNF-α, (F) IL-6 and (G) IL-1β in Caco-2 cells in the control, OGD/R (4 h) + si-NC and OGD/R (4 h) + si-*CTSB* groups. All data were obtained from at least three independent biological experiments (n=3). **P<0.01 vs. control; $^{\#}$P<0.05 vs. OGD/R (4 h) + si-NC. *CTSB*, cathepsin B; GSH-Px, glutathione peroxidase; MDA, malondialdehyde; NC, negative control; OGD/R, oxygen-glucose deprivation/reoxygenation; ROS, reactive oxygen species; si, small interfering; SOD, superoxide dismutase.

has emerged as a potential focal point for pharmacotherapy targeting I/R damage (21). Furthermore, in an I/R-induced mouse model, *TLR3* expression has been reported to be elevated in the intestinal mucosa, and its knockdown was found to reduce apoptosis of intestinal epithelial cells and lower levels of inflammatory cytokines post-I/R (22). Additionally, *TLR4* has been implicated in exacerbating I/R injury by augmenting the NF-κB signaling pathway (23). Although *CTSB* has been

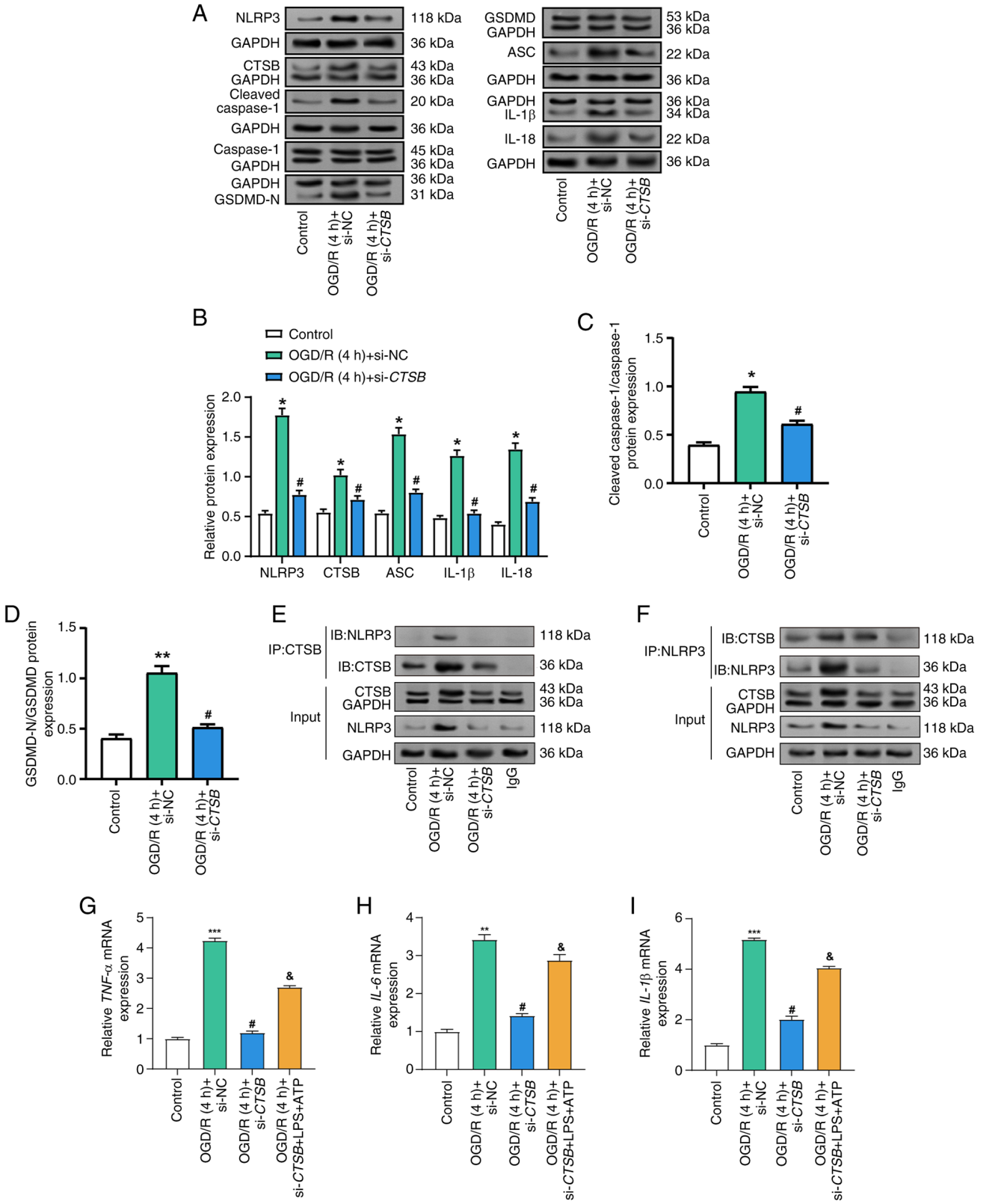

Figure 5. Knockdown of *CTSB* inhibits activation of the NLRP3 inflammasome in Caco-2 cells injured by OGD/R. (A) Representative WB analysis of inflammasome-related proteins in Caco-2 cells under control conditions, OGD/R (4 h) + si-NC and OGD/R (4 h) + si-*CTSB*. Each GAPDH blot shown corresponds to the target protein immediately above it. Semi-quantitative analysis of protein expression levels: (B) NLRP3, CTSB, ASC, IL-1β and IL-18; (C) cleaved caspase-1/caspase-1 ratio; and (D) GSDMD-N/GSDMD ratio. (E) Co-IP of CTSB and NLRP3 (IP: CTSB; IB: NLRP3 and CTSB). Inputs and IgG controls are shown. (F) Reciprocal co-IP (IP: NLRP3; IB: CTSB and NLRP3) confirming the interaction between CTSB and NLRP3 under OGD/R conditions. Reverse transcription-quantitative PCR detection of the relative mRNA expression levels of the cytokines (G) *TNF-α*, (H) *IL-6* and (I) *IL-1β* in Caco-2 cells in the control, OGD/R (4 h) + si-NC, OGD/R (4 h) + si-*CTSB* and OGD/R (4 h) + si-*CTSB* + LPS + ATP groups. All data were obtained from at least three independent biological experiments (n=3). *P<0.05, **P<0.01, ***P<0.001 vs. control; $^{\#}$P<0.05 vs. OGD/R (4 h) + si-NC; $^{\&}$P<0.05 vs. OGD/R (4 h) + si-*CTSB*. ATP, adenosine triphosphate; CTSB, cathepsin B; GSDMD, gasdermin D; GSDMD-N, cleaved N-terminal GSDMD; IB, immunoblot; IP, immunoprecipitation; LPS, lipopolysaccharide; NC, negative control; NLRP3, NLR family pyrin domain-containing 3; OGD/R, oxygen-glucose deprivation/reoxygenation; si, small interfering; WB, western blot.

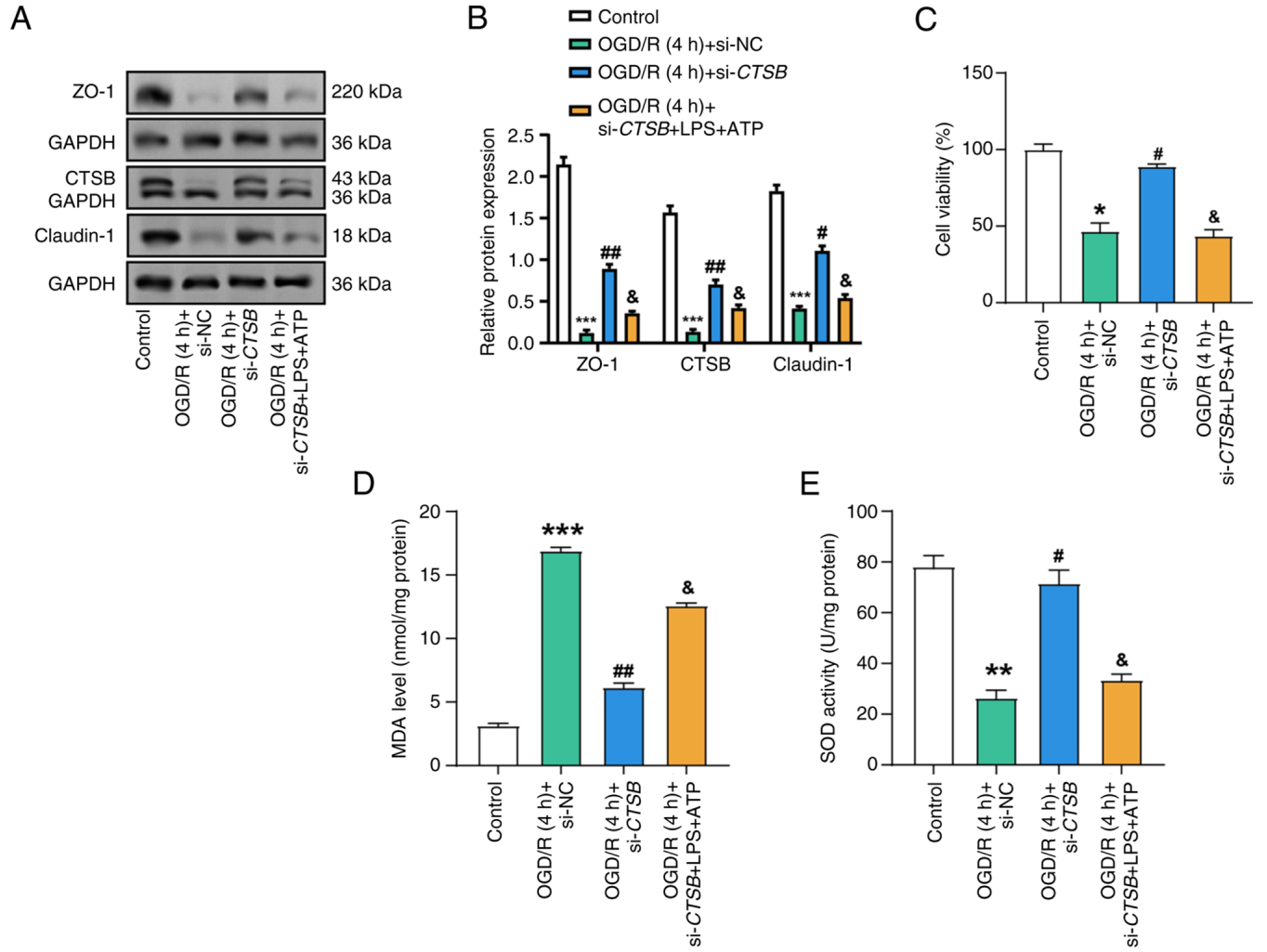

Figure 6. Effects of *CTSB* knockdown and LPS + ATP treatment on cell viability, oxidative stress and tight junction protein expression in OGD/R-treated Caco-2 cells. (A) Western blot analysis of the protein expression of CTSB, ZO-1 and claudin-1 in Caco-2 cells in the control, OGD/R (4 h) + si-NC, OGD/R (4 h) + si-*CTSB* and OGD/R (4 h) + si-*CTSB* + LPS + ATP groups, and (B) semi-quantitative analysis. (C) Cell Counting Kit-8 detected the viability of Caco-2 cells in the control, OGD/R (4 h) + si-NC, OGD/R (4 h) + si-*CTSB* and OGD/R (4 h) + si-*CTSB* + LPS + ATP groups. Detection of (D) MDA levels and (E) SOD activity in Caco-2 cells in the control, OGD/R (4 h) + si-NC, OGD/R (4 h) + si-*CTSB* and OGD/R (4 h) + si-*CTSB* + LPS + ATP groups. All data were obtained from at least three independent biological experiments (n=3). *P<0.05, **P<0.01, ***P<0.001 vs. Control. $^{\#}$P<0.05, $^{\#\#}$P<0.01 vs. OGD/R (4 h) + si-NC. $^{\&}$P<0.05 vs. OGD/R (4 h) + si-*CTSB* + LPS + ATP. ATP, adenosine triphosphate; CTSB, cathepsin B; LPS, lipopolysaccharide; MDA, malondialdehyde; NC, negative control; OGD/R, oxygen-glucose deprivation/reoxygenation; si, small interfering; SOD, superoxide dismutase.

recognized as a pivotal contributor to I/R injury in various organs, exacerbating renal I/R injury through apoptosis, inflammation and dysregulation of autophagy (24), and amplifying myocardial I/R inflammatory injury via the NLRP3 inflammasome (12), dedicated studies on its specific role in I/R injury remain sparse (25,26). Consequently, knowledge gaps persist regarding the regulatory mechanisms of *CTSB*, the breadth of its impact across diverse tissues and its potential as a therapeutic target. By conducting a comprehensive bioinformatics analysis, *CTSB* has been identified as a hub gene that is upregulated during I/R injury. Given the lack of research on *CTSB* in the context of I/R injury and its demonstrated capacity to mediate cellular responses during this process, *CTSB* was chosen as the focus of the current study. The objective of the study was to systematically and precisely elucidate its regulatory mechanisms, and to assess its influence on the pathophysiology of I/R injury, thereby addressing a crucial void in current research.

The lysosomal enzyme CTSB serves a pivotal role in regulating oxidative stress, inflammation and cell death (24). For example, in cells infected with a high dosage of *Legionella pneumophila*, knockdown of *CTSB* has been shown to effectively suppress cell death and inflammation (27). Prior research has also indicated that inhibiting *CTSB* can mitigate intestinal epithelial cell death and safeguard barrier function (10). Elevated *CTSB* levels have been reported to be associated with heightened inflammation and cellular damage in IBD (28). The *in vivo* process of I/R injury is frequently simulated using the OGD/R approach, which facilitates comprehension of the complex mechanisms underlying I/R damage, including oxidative stress, inflammation and apoptosis (29). The current study successfully replicated I/R-induced inflammation and intestinal barrier disruption in Caco-2 cells by employing the well-established OGD/R *in vitro* model. Caco-2 cells subjected to OGD/R exhibited decreased cell viability, disruption of tight junction proteins, increased LDH release, and elevated CTSB

protein levels and activity. Research has shown that IL-28A can protect the expression of occludin, ZO-1 and claudin-1, thereby enhancing the function of the epithelial barrier and reducing damage caused by intestinal I/R (30). A reduction in the expression of tight junction proteins can exacerbate inflammatory responses, augment vascular permeability and compromise tissue barrier function (31). These adverse effects were alleviated by *CTSB* knockdown, which also enhanced cell survival, diminished LDH release and restored tight junction protein levels. These findings suggest that *CTSB* knockdown may shield Caco-2 cells from damage induced by OGD/R. *CTSB* could thus serve as a key mediator of I/R-induced damage by diminishing cell viability and disrupting barrier proteins.

I/R injury is closely associated with oxidative stress, a pathological state characterized by an imbalance between the antioxidant defense mechanisms of the body and the generation of ROS (32). Within the framework of I/R, oxidative stress has been extensively studied, with compelling evidence indicating its pivotal role in tissue damage. For example, by promoting sirtuin 1-mediated suppression of epithelial ROS generation and apoptosis, the knockdown of miR-34a-5p has been shown to mitigate I/R-induced harm (33). Furthermore, oxidative stress indicators, such as MDA, SOD and GSH-Px, are commonly utilized to assess antioxidant capability and oxidative damage (34). Research has demonstrated that in I/R-injured cells, dexmedetomidine can alleviate oxidative stress by decreasing MDA levels and increasing SOD levels (35). Additionally, elevated GSH-Px activity in I/R injury can reduce oxidative stress, as it is often associated with enhanced antioxidant defense (36). Caco-2 cells originate from human colorectal adenocarcinoma but differentiate into enterocyte-like cells that form tight junctions and exhibit absorptive and barrier properties similar to intestinal epithelial cells (37,38). Therefore, in the current study, Caco-2 cells were selected as an *in vitro* model to investigate intestinal I/R injury. The present study explored how *CTSB* regulates oxidative stress in Caco-2 cells subjected to I/R injury. The OGD/R model revealed a significant elevation in cellular oxidative stress levels; however, this increase was attenuated by *CTSB* knockdown. These findings suggest the potential of *CTSB* as a therapeutic target to mitigate oxidative damage, implying its contribution to oxidative stress in I/R injury.

I/R injury exacerbates tissue damage and impedes the healing process by triggering a robust inflammatory response (1,39). The NLRP3 inflammasome, a multiprotein complex that is instrumental in activating inflammatory cytokines, serves as a crucial mediator of this inflammatory cascade (40). Numerous studies have identified the role of the NLRP3 inflammasome in I/R injury, with its activation leading to heightened inflammation and tissue damage (18,41). For example, *VX-765* has been shown to mitigate I/R-induced harm and alleviate oxidative stress by diminishing NLRP3 inflammasome activation (42). Additional research has highlighted the strong association between *CTSB* and the NLRP3 inflammasome (43). The activation of the NLRP3 inflammasome, which is induced by *CTSB*, along with the maturation of pro-inflammatory cytokines IL-1β and IL-18, can be significantly inhibited by Ilex saponin I (ISI) (25). Concurrently, by disrupting the CTSB/NLRP3 complex, ISI curtails the inflammatory response through inactivation of the NLRP3 inflammasome. According to Li *et al* (44), hollow cerium-oxide (CeO_2) nanospheres coated with non-stoichiometric copper oxide ($Cu_{5.4}O$) (abbreviated as $hCeO_2@Cu_{5.4}O$ nanoparticles) can reduce inflammation by modifying the CTSB-NLRP3 signaling pathway. The experimental findings of the current study demonstrated that the OGD/R model exhibited elevated levels of pro-inflammatory cytokines, and that *CTSB* knockdown markedly reduced these levels while obstructing NLRP3 inflammasome activation. These results underscore the pivotal role of *CTSB* in modulating NLRP3 inflammasome activation, offering promising therapeutic implications for alleviating I/R-induced intestinal inflammation. Notably, a direct interaction exists between CTSB and NLRP3, and it has been shown that CTSB can activate NLRP3 inflammatory vesicles through direct engagement with NLRP3 (45). This interaction may involve direct modification of NLRP3 by CTSB or may indirectly influence NLRP3 activity by altering the intracellular milieu. Additionally, the release of CTSB may activate the NLRP3 inflammasome via lysosomal rupture. In the current study, through co-IP experiments, the presence of a direct interaction between CTSB and NLRP3 was confirmed in an intestinal I/R model. This finding provides molecular-level evidence that CTSB may regulate its activity by directly interacting with NLRP3.

In the current study, it was observed that in *CTSB*-knockdown Caco-2 cells, the levels of inflammatory factors, such as TNF-α, IL-6 and IL-1β, were partially restored following LPS and ATP treatment. This observation suggests that while *CTSB* has a pivotal role in the inflammatory response induced by I/R injury, other regulators or pathways may circumvent the inhibitory effects of *CTSB* knockdown, thereby partially reinstating the inflammatory response. *CTSB* is crucial in I/R injury through its activation of the NLRP3 inflammasome, a process essential for the maturation of inflammatory factors, and CTSB can directly bind to NLRP3 and enhance its activity (11). In the present study, *CTSB* knockdown significantly suppressed OGD/R-induced NLRP3 inflammasome activation and inflammatory factor expression, further corroborating the key regulatory role of *CTSB* in I/R injury. LPS and ATP are well-established activators of the NLRP3 inflammasome, functioning through distinct signaling pathways. LPS activates NF-κB via the TLR4 signaling pathway, promoting the transcription of inflammatory factors (20). Conversely, ATP enters the cell through the P2X7 receptor and pannexin-1 channel, thereby activating the NLRP3 inflammasome (33). The partial recovery of inflammatory factors following LPS + ATP treatment in *CTSB*-knockdown cells may indicate that these alternative pathways can bypass the inhibitory effects of *CTSB* knockdown and reactivate the NLRP3 inflammasome. Although *CTSB* has a critical role in the inflammatory response, the recovery of inflammatory factors after LPS + ATP treatment suggests that *CTSB* may not be the sole regulator. The activation of the NLRP3 inflammasome involves multiple signaling pathways, including ROS generation, mitochondrial damage and lysosomal rupture (33). In the context of *CTSB* knockdown, other signaling pathways may be activated by LPS and ATP, thereby partially restoring the levels of inflammatory factors. For example, research has shown that ISI can inhibit the inflammatory response by

disrupting the CTSB/NLRP3 complex; however, this inhibition is not absolute, implying the existence of other compensatory mechanisms (40). This phenomenon does not undermine the significance of *CTSB* as a potential therapeutic target. Instead, it underscores the complexity of the inflammatory response and suggests that co-targeting multiple key molecules may be necessary to effectively inhibit the inflammatory response in clinical settings. For example, combined inhibition of *CTSB* and the TLR4 signaling pathway may prove more effective than inhibiting *CTSB* alone.

The present study was confined to *in vitro* experiments utilizing a Caco-2 cell model to simulate I/R injury. While *in vitro* models can offer valuable insights into the mechanism of action of *CTSB* in I/R injury, these findings necessitate further validation in *in vivo* models. For example, future investigations could employ mouse I/R models to assess the effects of *CTSB* knockdown or inhibition on intestinal injury, inflammatory response and oxidative stress. Such *in vivo* validation would aid in determining the clinical potential of *CTSB* as a therapeutic target. In the present study, despite *CTSB* knockdown significantly reducing the levels of inflammatory factors, these factors remained slightly elevated following LPS + ATP stimulation. This suggests that, in the absence of *CTSB*, other inflammasomes or alternative pathways may be activated, thus promoting the inflammatory response. Future studies are warranted to further explore these potential mechanisms, such as conducting a detailed analysis of the signaling pathways activated by LPS and ATP using specific inflammasome inhibitors or by knocking out other inflammasome components. Additionally, investigating the interaction between CTSB and other lysosomal enzymes or proteases may provide clues to understanding the compensatory mechanisms at play. It was hypothesized that the interaction between CTSB and NLRP3 may occur through multiple molecular mechanisms. CTSB may directly bind to NLRP3 and enhance the activity of the NLRP3 inflammasome, thereby promoting the maturation and release of inflammatory factors. Furthermore, CTSB may indirectly activate the NLRP3 inflammasome by affecting the integrity and function of lysosomes. However, a limitation of the current study is the lack of further verification regarding the specific details of CTSB activating NLRP3 through lysosomal rupture. Future studies may further verify this using advanced tools such as co-IP, mass spectrometry and lysosomal functional imaging techniques. Although the present study provides evidence for the critical role of *CTSB* in I/R injury, further research is needed to translate these findings into clinical applications. Future work should include validating the therapeutic effects of *CTSB* in *in vivo* models, and developing small-molecule inhibitors or gene therapy strategies targeting *CTSB*. Additionally, studying the role of *CTSB* in different tissues and cell types may help to devise more specific treatment options to reduce inflammation and tissue damage in I/R-related diseases.

In conclusion, the present study identified *CTSB* as a pivotal regulator of I/R-induced damage in Caco-2 cells, underscoring its critical role in intestinal barrier dysfunction, inflammation and oxidative stress. Notably, *CTSB* knockdown effectively mitigated cellular damage by reducing oxidative stress, restoring tight junction proteins and modulating NLRP3 inflammasome activation. Conversely, *CTSB* expression was significantly upregulated under OGD/R conditions. These findings elucidate how *CTSB* orchestrates inflammatory signals and influences intestinal barrier function during I/R injury.

Acknowledgements

Not applicable.

Funding

This study was funded by the Key Specialty Construction Project of the Pudong Health Commission of Shanghai (grant no. PWZzk2022-09) and the Qihang Project of Shanghai Pudong New Area People's Hospital (grant no. PRYQH202502).

Availability of data and materials

The data generated in the present study may be requested from the corresponding author.

Authors' contributions

SH, LW, ZW, HX and YW conceived and designed the research. SH, LW and ZW acquired the data. SH, LW, ZW, SY, QZ, YX and YJ analyzed and interpreted the data. SY, QZ, YX and YJ performed statistical analysis. SH, LW and ZW drafted the manuscript. HX and YW revised the manuscript for important intellectual content. SH and HX confirm the authenticity of all the raw data. All authors read and approved the final manuscript.

Ethics approval and consent to participate

Not applicable.

Patient consent for publication

Not applicable.

Competing interests

The authors declare that they have no competing interests.

References

1. Wang J, Zhang W and Wu G: Intestinal ischemic reperfusion injury: Recommended rats model and comprehensive review for protective strategies. Biomed Pharmacother 138: 111482, 2021.
2. Li G, Wang S and Fan Z: Oxidative stress in intestinal ischemia-reperfusion. Front Med (Lausanne) 8: 750731, 2022.
3. Zhang J, Liu Z, Liu Y, Shi Y, Chen F and Leng Y: Role of non-coding RNA in the pathogenesis of intestinal ischemia-reperfusion injury. Curr Med Chem 30: 4130-4148, 2023.
4. Li Y, Feng D, Wang Z, Zhao Y, Sun R, Tian D, Liu D, Zhang F, Ning S, Yao J and Tian X: Ischemia-induced ACSL4 activation contributes to ferroptosis-mediated tissue injury in intestinal ischemia/reperfusion. Cell Death Differ 26: 2284-2299, 2019.
5. Meng Q, Ye C and Lu Y: miR-181c regulates ischemia/reperfusion injury-induced neuronal cell death by regulating c-Fos signaling. Pharmazie 75: 90-93, 2020.
6. Zu G, Zhou T, Che N and Zhang X: Salvianolic acid A protects against oxidative stress and apoptosis induced by intestinal ischemia-reperfusion injury through activation of Nrf2/HO-1 pathways. Cell Physiol Biochem 49: 2320-2332, 2018.

7. Wu L, Xiong X, Wu X, Ye Y, Jian Z, Zhi Z and Gu L: Targeting oxidative stress and inflammation to prevent ischemia-reperfusion injury. Front Mol Neurosci 13: 28, 2020.
8. Hook G, Reinheckel T, Ni J, Wu Z, Kindy M, Peters C and Hook V: Cathepsin B gene knockout improves behavioral deficits and reduces pathology in models of neurologic disorders. Pharmacol Rev 74: 600-629, 2022.
9. De Pasquale V, Moles A and Pavone LM: Cathepsins in the pathophysiology of mucopolysaccharidoses: New perspectives for therapy. Cells 9: 979, 2020.
10. Hu ML, Liao QZ, Liu BT, Sun K, Pan CS, Wang XY, Yan L, Huo XM, Zheng XQ, Wang Y, *et al*: Xihuang pill ameliorates colitis in mice by improving mucosal barrier injury and inhibiting inflammatory cell filtration through network regulation. J Ethnopharmacol 319: 117098, 2024.
11. Dong L, Xie J, Wang Y, Jiang H, Chen K, Li D, Wang J, Liu Y, He J, Zhou J, *et al*: Mannose ameliorates experimental colitis by protecting intestinal barrier integrity. Nat Commun 13: 4804, 2022.
12. Liu C, Yao Q, Hu T, Cai Z, Xie Q, Zhao J, Yuan Y, Ni J and Wu QQ: Cathepsin B deteriorates diabetic cardiomyopathy induced by streptozotocin via promoting NLRP3-mediated pyroptosis. Mol Ther Nucleic Acids 30: 198-207, 2022.
13. Zhao S, Gong Z, Zhou J, Tian C, Gao Y, Xu C, Chen Y, Cai W and Wu J: Deoxycholic acid triggers NLRP3 inflammasome activation and aggravates DSS-induced colitis in mice. Front Immunol 7: 536, 2016.
14. Liu M, Wen H, Zuo L, Song X, Geng Z, Ge S, Ge Y, Wu R, Chen S, Yu C and Gao Y: Bryostatin-1 attenuates intestinal ischemia/reperfusion-induced intestinal barrier dysfunction, inflammation, and oxidative stress via activation of Nrf2/HO-1 signaling. FASEB J 37: e22948, 2023.
15. Zhao Y, Zhuang Y, Shi J, Fan H, Lv Q and Guo X: Cathepsin B induces kidney diseases through different types of programmed cell death. Front Immunol 16: 1535313, 2025.
16. Kip AM, Grootjans J, Manca M, Hadfoune MH, Boonen B, Derikx JPM, Biessen EAL, Olde Damink SWM, Dejong CHC, Buurman WA and Lenaerts K: Temporal transcript profiling identifies a role for unfolded protein stress in human gut ischemia-reperfusion injury. Cell Mol Gastroenterol Hepatol 13: 681-694, 2022.
17. Livak KJ and Schmittgen TD: Analysis of relative gene expression data using real-time quantitative PCR and the 2(-Delta Delta C(T)) method. Methods 25: 402-408, 2001.
18. Wang Z, Li Z, Feng D, Zu G, Li Y, Zhao Y, Wang G, Ning S, Zhu J, Zhang F, *et al*: Autophagy induction ameliorates inflammatory responses in intestinal Ischemia-reperfusion through inhibiting NLRP3 inflammasome activation. Shock 52: 387-395, 2019.
19. Nadatani Y, Watanabe T, Shimada S, Otani K, Tanigawa T and Fujiwara Y: Microbiome and intestinal ischemia/reperfusion injury. J Clin Biochem Nutr 63: 26-32, 2018.
20. Zhenzhen L, Wenting L, Jianmin Z, Guangru Z, Disheng L, Zhiyu Z, Feng C, Yajing S, Yingxiang H, Jipeng L, *et al*: miR-146a-5p/TXNIP axis attenuates intestinal ischemia-reperfusion injury by inhibiting autophagy via the PRKAA/mTOR signaling pathway. Biochem Pharmacol 197: 114839, 2022.
21. Cong R, Yang J, Zhou J, Shi J, Zhu Y, Zhu J, Xiao J, Wang P, He Y and He B: The potential role of protein tyrosine phosphatase, receptor type C (CD45) in the intestinal ischemia-reperfusion injury. J Comput Biol 27: 1303-1312, 2020.
22. Zhang XY, Liang HS, Hu JJ, Wan YT, Zhao J, Liang GT, Luo YH, Liang HX, Guo XQ, Li C, *et al*: Ribonuclease attenuates acute intestinal injury induced by intestinal ischemia reperfusion in mice. Int Immunopharmacol 83: 106430, 2020.
23. Yang J, Wu Y, Xu Y, Jia J, Xi W, Deng H and Tu W: Dexmedetomidine resists intestinal ischemia-reperfusion injury by inhibiting TLR4/MyD88/NF-κB signaling. J Surg Res 260: 350-358, 2021.
24. Liu C, Cai Z, Hu T, Yao Q and Zhang L: Cathepsin B aggravated doxorubicin-induced myocardial injury via NF-κB signalling. Mol Med Rep 22: 4848-4856, 2020.
25. Wu J, Chen S, Wu P, Wang Y, Qi X, Zhang R, Liu Z, Wang D and Cheng Y: Cathepsin B/HSP70 complex induced by Ilexsaponin I suppresses NLRP3 inflammasome activation in myocardial ischemia/reperfusion injury. Phytomedicine 105: 154358, 2022.
26. Sun C, Cao N, Wang Q, Liu N, Yang T, Li S, Pan L, Yao J, Zhang L, Liu M, *et al*: Icaritin induces resolution of inflammation by targeting cathepsin B to prevents mice from ischemia-reperfusion injury. Int Immunopharmacol 116: 109850, 2023.
27. Morinaga Y, Yanagihara K, Nakamura S, Hasegawa H, Seki M, Izumikawa K, Kakeya H, Yamamoto Y, Yamada Y, Kohno S and Kamihira S: Legionella pneumophila induces cathepsin B-dependent necrotic cell death with releasing high mobility group box1 in macrophages. Respir Res 11: 158, 2010.
28. Menzel K, Hausmann M, Obermeier F, Schreiter K, Dunger N, Bataille F, Falk W, Scholmerich J, Herfarth H and Rogler G: Cathepsins B, L, and D in inflammatory bowel disease macrophages and potential therapeutic effects of cathepsin inhibition in vivo. Clin Exp Immunol 146: 169-180, 2006.
29. Liu Y, Ji T, Jiang H, Chen M, Liu W, Zhang Z and He X: Emodin alleviates intestinal ischemia-reperfusion injury through antioxidant stress, anti-inflammatory responses, and anti-apoptosis effects via Akt-mediated HO-1 upregulation. J Inflamm (Lond) 21: 25, 2024.
30. Li L, Zhou C, Li T, Xiao W, Yu M and Yang H: Interleukin-28A maintains the intestinal epithelial barrier function through regulation of claudin-1. Ann Transl Med 9: 365, 2021.
31. Brooks TA, Hawkins BT, Huber JD, Egleton RD and Davis TP: Chronic inflammatory pain leads to increased blood-brain barrier permeability and tight junction protein alterations. Am J Physiol Heart Circ Physiol 289: H738-H743, 2005.
32. Adwas AA, Elsayed A, Azab AE and Quwaydir FA: Oxidative stress and antioxidant mechanisms in human body. J Appl Biotechnol Bioeng 6: 43-47, 2019.
33. Wang G, Yao J, Li Z, Zu G, Feng D, Shan W, Li Y, Hu Y, Zhao Y and Tian X: miR-34a-5p inhibition alleviates intestinal ischemia/reperfusion-induced reactive oxygen species accumulation and apoptosis via activation of SIRT1 signaling. Antioxid Redox Signal 24: 961-973, 2016.
34. Li F, Wang X, Deng Z, Zhang X, Gao P and Liu H: Dexmedetomidine reduces oxidative stress and provides neuroprotection in a model of traumatic brain injury via the PGC-1α signaling pathway. Neuropeptides 72: 58-64, 2018.
35. Hou M, Chen F, He Y, Tan Z, Han X, Shi Y, Xu Y and Leng Y: Dexmedetomidine against intestinal ischemia/reperfusion injury: A systematic review and meta-analysis of preclinical studies. Eur J Pharmacol 959: 176090, 2023.
36. Ustundag B, Kazez A, Demirbag M, Canatan H, Halifeoglu I and Ozercan IH: Protective effect of melatonin on antioxidative system in experimental ischemia-reperfusion of rat small intestine. Cell Physiol Biochem 10: 229-236, 2000.
37. Sambuy Y, De Angelis I, Ranaldi G, Scarino M, Stammati A and Zucco F: The Caco-2 cell line as a model of the intestinal barrier: Influence of cell and culture-related factors on Caco-2 cell functional characteristics. Cell Biol Toxicol 21: 1-26, 2005.
38. Meunier V, Bourrie M, Berger Y and Fabre G: The human intestinal epithelial cell line Caco-2; pharmacological and pharmacokinetic applications. Cell Biol Toxicol 11: 187-194, 1995.
39. Deng F, Lin ZB, Sun QS, Min Y, Zhang Y, Chen Y, Chen WT, Hu JJ and Liu KX: The role of intestinal microbiota and its metabolites in intestinal and extraintestinal organ injury induced by intestinal ischemia reperfusion injury. Int J Biol Sci 18: 3981, 2022.
40. Moretti J and Blander JM: Increasing complexity of NLRP3 inflammasome regulation. J Leukoc Biol 109: 561-571, 2021.
41. Ito H, Kimura H, Karasawa T, Hisata S, Sadatomo A, Inoue Y, Yamada N, Aizawa E, Hishida E, Kamata R, *et al*: NLRP3 inflammasome activation in lung vascular endothelial cells contributes to intestinal ischemia/reperfusion-induced acute lung injury. J Immunol 205: 1393-1405, 2020.
42. Lyu H, Ni H, Huang J, Yu G, Zhang Z and Zhang Q: VX-765 prevents intestinal ischemia-reperfusion injury by inhibiting NLRP3 inflammasome. Tissue Cell 75: 101718, 2022.
43. Cai Z, Xu S and Liu C: Cathepsin B in cardiovascular disease: Underlying mechanisms and therapeutic strategies. J Cell Mol Med 28: e70064, 2024.
44. Li Y, Xia X, Niu Z, Wang K, Liu J and Li X: hCeO2@ Cu5.4O nanoparticle alleviates inflammatory responses by regulating the CTSB-NLRP3 signaling pathway. Front Immunol 15: 1344098, 2024.
45. Xu W, Huang Y and Zhou R: NLRP3 inflammasome in neuroinflammation and central nervous system diseases. Cell Mol Immunol 22: 341-355, 2025.